Steel and Composite Structures, *Vol. 22, No. 6 (2016) 1337-1358*
DOI: http://dx.doi.org/10.12989/scs.2016.22.6.1337

Investigation of interface response of reinforced concrete columns retrofitted with composites

Dimitra V. Achillopoulou *, Alexandra N. Kiziridou, Georgios A. Papachatzakis and Athanasios I. Karabinis

Reinforced Concrete Laboratory, Civil Engineering Department, Democritus University of Thrace (D.U.Th.), Vas. Sofias 12, 67100, Xanthi, Greece

(*Received April 22, 2016, Revised November 10, 2016, Accepted November 24, 2016*)

Abstract. The current study focuses on the assessment and interface response of reinforced concrete elements with composite materials (carbon fiber reinforced polymers-CFRPs, glass fiber reinforced polymers-GFRPs, textile reinforced mortars-TRM's, near surface mounted bars-NSMs). A description of the transfer mechanisms from concrete elements to the strengthening materials is conducted through analytical models based on failure modes: plate end interfacial debonding and intermediate flexural crack induced interfacial debonding. A database of 55 in total reinforced concrete columns (scale 1:1) is assembled containing elements rehabilitated with various techniques (29 wrapped with CFRP's, 5 wrapped with GFRP's, 4 containing NSM and 4 strengthened with TRM). The failure modes are discussed together with the performance level of each technique as well as the efficiency level in terms of ductility and bearing/ bending capacity. The analytical models' results are in acceptable agreement with the experimental data and can predict the failure modes. Despite the heterogeneity of the elements contained in the aforementioned database the results are of high interest and point out the need to incorporate the analytical expressions in design codes in order to predict the failure mechanisms and the limit states of bearing capacities of each technique.

Keywords: concrete column; retrofit; fiber reinforced polymers; interface; force transfer mechanism

1. Introduction

Composites over the past years are proved to play an important role on the strengthening of existing structures especially under the prism of modern ductile regulations. Many investigations have been conducted considering the kind of composite used (GFRP, CFRP), the type of the added element (jacket, NSM rods, laminates, TRM) and above all its efficiency to enhance the response of the rehabilitated structural element made of reinforced concrete. (Elwan and Omar 2014, Panda *et al*. 2012, Su *et al*. 2016).

Even though modern codes internationally have incorporated various expressions in order to help the new practitioners to perform safe design, there is a lack of instructions considering which method is more appropriate for every different scenario. In fact, many standards and codes describe techniques and response without emphasizing on the failure modes of each rehabilitation

*Corresponding author, Dr., M.Sc. Civil Engineer, E-mail: dimiachi@civil.duth.gr

Copyright © 2016 Techno-Press, Ltd.
 ISSN: 1229-9367 (Print), 1598-6233 (Online)

system based on performance criteria.

Previous studies have focused on the investigation of various variables which affect the overall response of structural elements such as: confinement, flexural and torsional response, axial load capacity, cross-section shape, kind of loading, lap-splices existence, bar buckling phenomena, contribution of others structural elements, etc. (Chalioris 2008, Karabinis 2002, Karayannis and Sirkelis 2008, Rousakis *et al*. 2007).

In cases of vertical elements the loading conditions which include both axial and shear load- even with reversed sign/ cyclic load- simulate a more realistic specimen of full scale (1:1) which actually can be considered as a concrete column part of a real structure. In the presence of both loads the efficiency of each strengthening system is affected.

The approach of this study aims primarily to the investigation of the interface performance of each technique. As it is world widely admitted to be the key element of safe design and chained to failure modes, a deeper understanding of every failure mode and the divergence of codes' provisions is fundamental. Within this ambit, a cautious collection of experimental data and analytical expressions have been gathered. Here it follows a brief review of literature to help define the problem and set the variables.

Especially in rectangular or square cross-sections new techniques like embedment of lateral bars made of composite materials acting as anchors placed on each side can act favorably on augmenting the displacement ductility and energy dissipation. This technique has also proven to prevent longitudinal rebars from buckling and concrete deterioration (Wu *et al*. 2008).

A new approach by using the new material textile reinforcement mortar (TRM) in columns with or without lap-splices showed remarkable results. Columns without lap-splices exhibited higher energy dissipation- 50% higher- and drift ratio if compared to columns of the same stiffness level strengthened with FRPs. It was noticed that the lap-splices length is an important factor. In cases of TRM strengthening with short length of lap-splices the response was sufficient though lower compared to FRP strengthening systems. These results are also in accordance with EN 1998-3 (2005) (EC8). These provisions are excellent in cases of lack or short lap-splices (Bournas *et al*. 2009). In fact, authors noted that this kind of strengthening technique dislocated failure away from the possible plastic hinge sections, that is no failure of interface of FRP and concrete.

Sarafaz and Danesh (2010) applied the system of NSM rods together with FRP confinement on full scale square concrete columns subjected to both axial and cyclic horizontal loads. In this case, not only flexural response was improved but also the dissipation of energy and displacement ductility. The augmentation of ductility prevents NSM instability under compression and crack patterns development under tension when combined with FRP wrapping.

The importance of confinement with the new tendency of strap wrapping was investigated by Realfonzo and Napoli (2009). They investigated concrete columns confined with FRPs acting together with steel profiles placed at the corners. The kind of rebars was set as a variable (smooth, deformed rebars) affecting the results in terms of flexural capacity, energy dissipation and displacement ductility. Moreover, the role of axial load was crucial for failures.

By following the preliminary studies Realfonzo and Napoli (2012) investigated on the important factor of cross-section shape. They took into consideration the high aspect ratio of cross-sections very often met in reinforced concrete elements. They applied the simple case of CFRP jackets on columns containing smooth or deformed steel rebars but also adding cold bent steel profiles. For these cases they noted higher flexural strength combined with small ductility reduction caused by debonding. Due to this kind of failure the proposed manufacturer's deformation was not achieved.

Sadone *et al*. (2012) studied rectangular columns subjected to seismic loading and strengthened with CFRP sheets and composite laminates placed along the specimens' height. The composite plates did not seem to contribute significantly in the overall response of the columns, while confinement with CFRP sheets proved to help in terms of deformation ductility.

By looking at the interface study there is a gap of knowledge considering interfacial forces and transferring. Especially, a description that can predict the type of the upcoming failure with the desired response. Analytical research is limited mainly to concrete beams (Hadji *et al*. 2016, Smith and Teng 2001, Wang 2006, 2007, Wang and Zhang 2008). These studies describe mainly two kind of failures: a) plate end debonding, b) intermediate crack induced by external loading.

Smith and Teng (2001) developed their model primarily under the assumption that the interfacial stresses do not vary across the adhesive layer thickness. Except for that, they simplified calculations by neglecting shear deformations. The proposed model is mainly orientated for applications in which stiffness of beam and composite are relatively comparable.

In literature three different approaches exist:

(a) Material's strength method
(b) Linear elastic fracture mechanics (LEFM) method and
(c) Non-linear fracture mechanics (cohesive zone model)

The cohesive zone model (Smith and Teng 2001) gains more and more attention since it takes into account the microscopic details that cause energy dissipation. This method was proved to be effective apart from efficient to describe the mixed-mode debonding based on energy release (Wang 2006). Following research of the same authors (Wang and Zhang 2008) a useful description of flexural-shear crack induced interfacial debonding of FRP in strengthened concrete beams is found.

The objectives of this study is mainly to clarify the interface results of a wide research on strengthened full scale concrete columns with composite elements which are found in literature by many researchers. In this way, the effectiveness of each strengthening system is evaluated, in enhancing displacement ductility, strength and the performance of the columns on the whole. For these reasons a wide dataset with results of various researchers is collected and statistical tools are used to evaluate and discuss the results.

The specimens were subjected to horizontal cyclic loading with constant axial load. The conclusions of this research are presented after analyzing and processing the results. Furthermore, provisions of design codes (EN 1998-3 2005, CNR 2004, *fib*-Bulletin No. 56 2010) were used in order to be evaluated, based on statistical comparison of displacement ductility of the aforementioned elements.

Finally, a simple algorithm based on previous research describes the effectiveness of an FRP jacket wrapped to a concrete column in order to understand better the slip phenomena and the effective zone of the jacket- substrate system and the failure of interface. The effectiveness of externally bonded fiber reinforced polymer (FRP) composites to strengthened concrete components depends intrinsically on bond and transfer related aspects. Premature debonding, initiated from ends or from cracks in the concrete, often limits potential performance gains. The current study aims to examine and analytically investigate the force transfer mechanism at the interface of columns reinforced with FRP jackets that are subjected to bending and compressive external forces. Relative slippage at the interface occurs at the point where bending cracks are created (due to the high moment caused at the base of the columns by the horizontal load imposed on the top), resulting in risk of debonding. In order to understand this phenomenon, analytical

equations implementing non-linear slip- stress law for the calculation of internal stresses (shear and normal) along the interface of the column for a certain load level were developed for calculating the ultimate load in which debonding occurs.

2. Experimental results

2.1 Database

A database containing results of 55 experimental tests performed on square and rectangular, full scale elements was assembled from the scientific literature (Wu *et al*. 2008, Bournas *et al*. 2009, Sarafaz and Danesh 2010, Realfonzo and Napoli 2009, 2012, Sadone *et al*. 2012). All the specimens were subjected to cyclic loading and a constant axial load. Of these, 42 columns were retrofitted with composite materials; 33 were reinforced with CFRP, 2 with GFRP, 2 with NSM, 1 with transverse embedded GFRP bars placed in the middle of each side of the column, 3 with carbon textile reinforced mortar (TRM C) and 1 with glass textile reinforced mortar (TRM G). Some of the specimens with CFRP sheet reinforcement were designed with additional retrofitting; 2 included NSM bars, 2 included embedded GFRP bars and 1 included CFRP laminates. The columns were designed either with smooth (18 specimens) either with deformed (37 specimens) longitudinal reinforcement. Furthermore, 38 of the experiments included lap-splices.

2.2 Codes

Provisions of design codes (EN 1998-3 2005, CNR 2004, *fib*-Bulletin No. 56 2010) were evaluated using the database regarding ductility accomplished through each strengthening technique. Displacement ductility was calculated according to each design code's provision, using the equations listed below.

For every code displacement ductility μ_δ was considered equal to chord rotation ductility, which is calculated by the following equation

$$\mu_\delta = \mu_\theta = \frac{\theta_u}{\theta_y} \tag{1}$$

where θ_u is the ultimate chord rotation and θ_y is the chord rotation at yielding.

The ultimate chord rotation for EN 1998-3 (2005) (EC8) is estimated according to equations in §A.3.2.2 and the chord rotation at yielding according to equations in §A.3.2.4.

Respectively, θ_u and θ_y is calculated by equations (4.54) and (4.55) in §4.7.3.1.2 for Italian design code CNR (2004).

As for chord rotations according to *fib*'s Bulletin provisions (*fib*-Bulletin No. 56 2010), θ_u is estimated by equation (7.4-40) in §7.4.3.4 and θ_y by provisions in §7.4.3.2.1.

3. Evaluation of strengthening method

3.1 Evaluation indexes

Several indexed were formed in order to evaluate the results with more accuracy.

The normalized bending moment is given by Eq. (2)

$$\mu_{\max} = \frac{F_{\max} * H}{b * h^2 * f_{cm}} \tag{2}$$

where $F_{\max}$ is the maximum lateral load, H is the height of the specimen, h and b are the height and width of the specimen's section and f_{cm} is the concrete's mean compressive strength.

The improvement in terms of flexural strength and deformation capacity has been evaluated by means of the following two indexes:

The flexural strength index I_μ which is described by Eq. (3)

$$\mathrm{I}_\mu = \frac{\mu_{\max}}{\mu_{\max,un}} \tag{3}$$

and the maximum displacement index I_δ which is given by Eq. (4)

$$\mathrm{I}_\delta = \frac{\delta_{\max}}{\delta_{\max,un}} \tag{4}$$

where $\mu_{\max}$ and $\mu_{\max,un}$ are the normalized bending moments and $\delta_{\max}$ and $\delta_{\max,un}$ are the maximum displacements of the column and the corresponding unstrengthened specimen, respectively.

Furthermore, the displacement index, in which the first failure is noted I_δ^1, is used in order to understand the level of displacement developed when the column is retrofitted (Eq. (5)). The first failure corresponds to the first noticeable failure (FRP failure, concrete crush, concrete spalling, bar buckling, NSM and concrete crush, NSM debonding, slippage or pullout of steel connectors) of each specimen.

$$\mathrm{I}_\delta{}^1 = \frac{\delta_1}{\delta_{1,un}} \tag{5}$$

where δ_1 and $\delta_{1,un}$ are the specimen's and the corresponding unstrengthened column's displacement in which the first failure is formed.

The increase in terms of confined concrete strength is represented by the index f'_{cc}/f_{cc}, where f_{cc} is the confined concrete's compressive strength due to transverse steel reinforcement confinement and f'_{cc} is the confined concrete's compressive strength due to transverse steel and composite material reinforcement confinement.

Drift ratio (Eq. (6)) is also a useful index since it shows the displacement capacity normalized to the column's height.

$$dr = \frac{\delta_1}{H} \tag{6}$$

3.2 Statistical indexes

In statistics, the coefficient of determination, denoted R^2, is a number that indicates how well data fit a statistical model. In regression, the coefficient of determination R^2 (Eq. (7)) is a statistical measure of how well the regression line approximates real data points. An R^2 equal to 1 indicates that the regression line perfectly fits the data, while an R^2 of 0 indicates that the line does not fit the data at all. This latter can be because the data is non-linear or because it is random.

$$R^2 = \left(\frac{Cov\ (exp, d)}{S(exp) * S(d)}\right)^2 \quad (7)$$

where d is the corresponding design code's value.

The root of the mean squared error *RMSE* (Eq. (8)) is a measure of the dispersion of the distribution of predicted results' errors. In other words, it calculates the root of the mean squared deviations of the predicted values from the respective experimental. Root Mean Squared Error (*RMSE*) and data are of the same scale and its' main characteristic is that it is more sensitive to extreme values, values that are far from the mean of errors. The smaller the value of *RMSE* index is, the more reliable are the results of prediction of ductility from provisions of the design codes used.

$$RMSE = \sqrt{\frac{\sum(\mu_{\delta,exp} - \mu_{\delta,d})^2}{n}} \quad (8)$$

Due to lack of data for certain type of failures, conclusions from R^2 and *RMSE* were drawn for FRP fracture and concrete spalling failures that the majority of specimens noted.

3.3 Analytical investigation, assumptions and approach

The effectiveness of externally bonded fiber reinforced polymer (FRP) composites to strengthen concrete depends intrinsically on bond and transfer related aspects. Premature debonding, initiated from ends or from cracks in the concrete, often limits potential performance gains. The current study aims to examine and analytically investigate the force transfer mechanism at the interface of columns reinforced with FRP jackets that are subjected to horizontal and axial compressive loads. Relative slippage at the interface occurs at the point where bending cracks are created (due to the high level of moment stress at the base of the columns by the horizontal load imposed on the top), resulting in risk of debonding. In order to describe this phenomenon, analytical equations for the calculation of internal stresses (shear and normal) along the interface of the column were developed for calculating the ultimate load in which debonding occurs. It's worth noticing that we consider the curvature caused by bending is the dominant mechanism for debonding of the FRP. In fact, the compressive axial load acting on columns doesn't provoke a shear stress higher than the bonding stress of the resin. As such, tension of the reversal horizontal load is the main component for the stress flow on the interface. Previous research has used the principle of reciprocity to describe similar complexed phenomena (Chalioris 2007) and have pointed out the contribution of the crack pattern in debonding (Chen and Teng 2003). The relative slip between the FRP and the substrate is dependent on the crack width which is significant for bending and shear cracks. In fact, the inclination of those kind of cracks affect the stress flow as have well documented the previous researchers and codes.

Both columns and the fiber reinforced polymers are modelled as linear elastic members connected by a thin layer of binding material. The flexural crack introduces local flexibility at the crack location (at the bottom of the column) and is conventionally modelled as a rotational spring with infinitesimal thickness at the crack location. The basic assumption in all of these solutions is that the adhesive layer is subjected to shear and normal stresses which are considered as constant.

A series of focused experiments (Bizindavyi and Neale 1999, Chajes *et al*. 1996) show that local interfacial shear stress distribution (mode II fracture behaviour), effective bond length, and

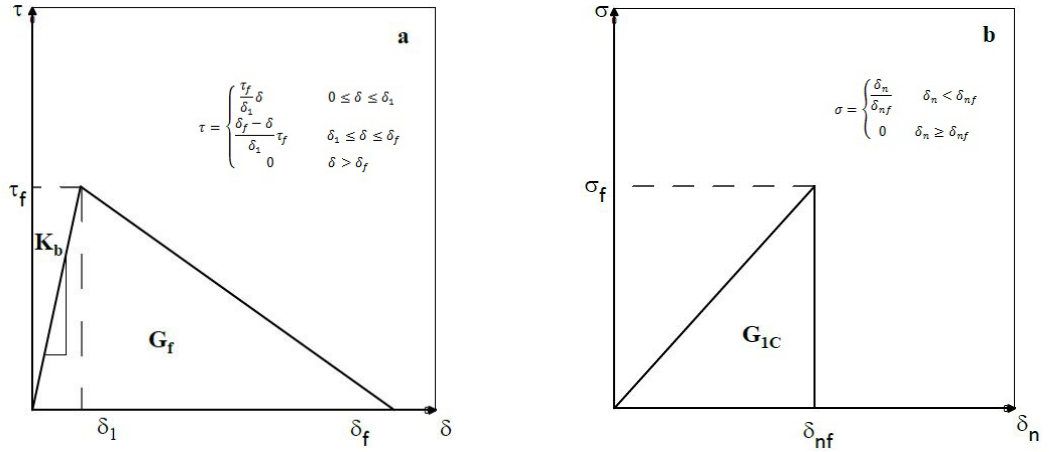

(a) Interfacial shear stress–slip relationship (b) Interfacial normal stress–displacement relationship

Fig. 1 Schematic representation of FRP–concrete bond behavior

initiation and propagation of an interfacial crack between the bonded FRP and concrete can be described fairly accurately by using a linear softening shear stress–slip relationship consisting of linearly ascending and descending branches as shown in Fig. 1(a). Bond stress increases linearly with an increase in relative shear displacement until the local bond strength, τ_f, is reached (*Stage I*: *Linearly Elastic Stage*) (Fig. 2(a)) and the shear stress along the column's interface counting from the column base is given by

$$\tau(x) = Ae^{-\lambda_1 x} + Be^{\lambda_1 x} + \tau_c \tag{9}$$

Where A, B are constants depending on geometrical characteristics of the concrete column and FRP, λ_1 is derived from the values of shear stress-bond slip laws values (Fig. 1(a)) and τ_c is essentially the shear stress along the FRP–concrete interface if the FRP–concrete system is treated as a fully composite column.

Let's assume that the external load level is high enough to cause the shear stress value above τ_f. In such a case part of the interface turns to soften. In this Elastic Softening Stage (*Stage II*: *Elastic-softening stage*) (Fig. 2(a)) two sub-regions along the interface are formed until complete loss of bonding: (a) Sub-region I considering the linear elastic sub-region ($\delta \le \delta_1$) in which the solution of shear stress has the same form as in Eq. (9) as shown in Eq. (10)

$$\tau^e(x) = A_1 e^{-\lambda_1 (x-a)} + \tau_c \tag{10}$$

where α is the softening zone size and coefficient A_1 is determined by the boundary condition

$$\tau^e|_{x=\alpha} = \tau_f \tag{11}$$

and (b) Sub-region II considering the Linearly Softening sub-region ($\delta_1 < \delta \le \delta_f$) expressed by (Eq. (12))

$$\tau^s(x) = C\cos\big(\lambda_2(x-a)\big) + D\sin\big(\lambda_2(x-a)\big) + \tau_c \tag{12}$$

where C, D are two coefficients determined by continuous conditions at $x = a$ and λ_2 is derived from the values of shear stress-bond slip laws values (Fig. 1(a)).

Finally, if the external horizontal load is high enough for shear stress to reach the debonding limit, full debonding occurs along the interface and propagates in a distance d from the location of the flexural crack. In this region, the interface shear stress is zero. In this stage (*Stage III*: *Elastic-Softening-Debonding Stage*) (Fig. 2(c)), the interface is divided in three sub-regions. The stress distribution within Sub-region *I* and *II* can be obtained by simply shifting d in abscissa in that of elastic-softening stage. The shear stress can be expressed in this stage as

$$\tau^e(x) = A_1 e^{-\lambda_1(x-d-a)} + \tau_c(x) \tag{13}$$

$$\tau^s(x) = C\cos\big(\lambda_2(x-d-a)\big) + D\sin\big(\lambda_2(x-d-a)\big) + \tau_c(x) \tag{14}$$

$$\tau(x) = 0 \tag{15}$$

where $\tau^e(x)$ is referred to the Elastic sub-region of the interface (Sub-*region I*), $\tau^s(x)$ is the Softening sub-region (Sub-r*egion II*). Finally, in *Sub-region III* the shear stress is zero.

Horizontal and axial loads create relative slip along the interface on the vertical axis of the elements. Lateral relative movement between the two interfaces appears (*Type I Fault*) (Fig. 1(b)). This separation creates normal stresses along the interface (Smith and Teng 2001, Wang 2007), which can be expressed by the relationship

$$\sigma(x) = b_2 \frac{\sigma_f}{\delta_{nf}}(w_2 - w_1) = K_n(w_2 - w_1) \tag{16}$$

After proper derivations the normal stress along the column is calculated by

$$\sigma(x) = e^{-\beta x}\left[C_1 \cos(\beta x) + C_2 \sin(\beta x)\right] + n_1 * \tau(x)' \tag{17}$$

where β is constant derived from interfacial normal stress–displacement relationship values (Fig. 1(b)) and C_1, C_2 are calculated from boundary conditions. Constant n_1 has different expressions at different sub-regions of the interface (Fig. 2).

Debonding occurs when no stress can be transferred, or when the energy required to create a unit area of debond is available. The area under the curve determines the interfacial fracture energy, G_{if}.

The tensile strength of adhesive is significantly greater than the concrete tensile strength. As such debonding often occurs within the cover concrete. So mode I fracture behavior at the interface can be assumed to follow that of concrete as shown in (Fig. 1(b)). It should be noticed that no account is taken of the coupling effect between mode I and mode II behavior other than the assumption that no shear transfer occurs along the interface once the magnitude of peeling stress attains the level of the concrete tensile strength, f_t, or enters the softening branch. Thus, loss of shear transfer capacity can occur if either mode II fracture energy G_{if} is met, or if the normal tensile stress, f_t, is attained.

3.4 Internal interface stresses and debonding failure mechanism

Given the geometrical and mechanical characteristics of the column and the fiber reinforced

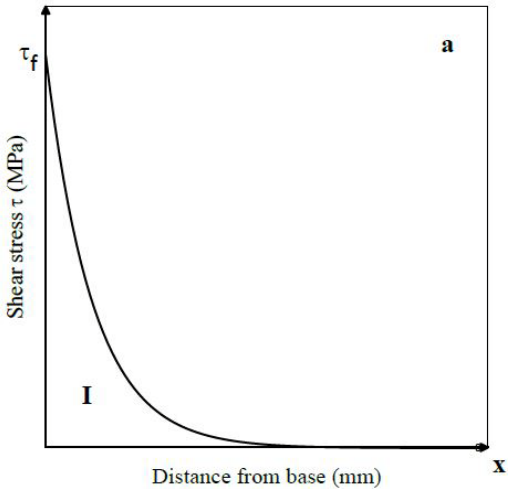

(a) Stage I: Linearly elastic stage

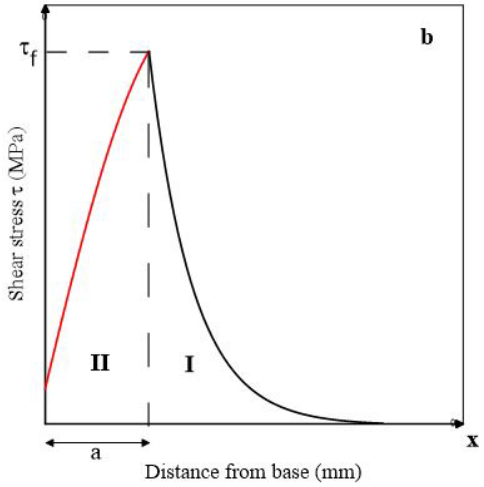

(b) Stage II: Elastic-softening stage

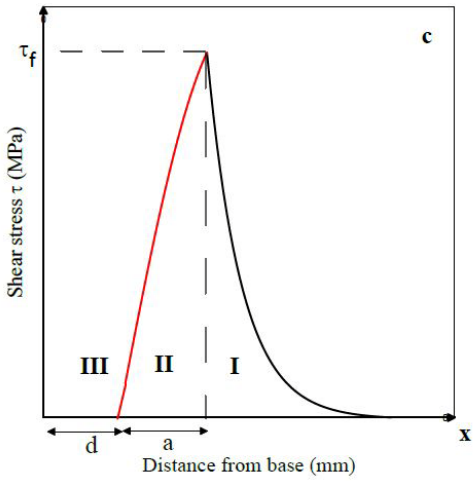

(c) Stage III: Elastic-softening-debonding stage

Fig. 2 Shear stress along the concrete interface

polymers used for the retrofitting and the required values to describe the interfacial shear stress/normal stress–slip relationship (Fig. 1), an iterative process can be used to obtain the following: (i) external load P_e: where the interface is in the elastic zone (Stage I: Linearly elastic stage); (ii) maximum external load P_u after which debonding occurs, thus the specimen loses shear transfer capacity and concrete is separated from FRP in the interface leading to failure (Stage III: Elastic-softening-debonding stage) (Fig. 3). After calculating interface capacity, the internal stresses (shear and normal) along the column-FRP interface can be obtained, by using the analytical equations for a certain given external load. Finally, taking account the values of the forces acting on the interface, any other failures related to the interface behavior (concrete's substrate failure, FRP fracture), can be observed (Fig. 4).

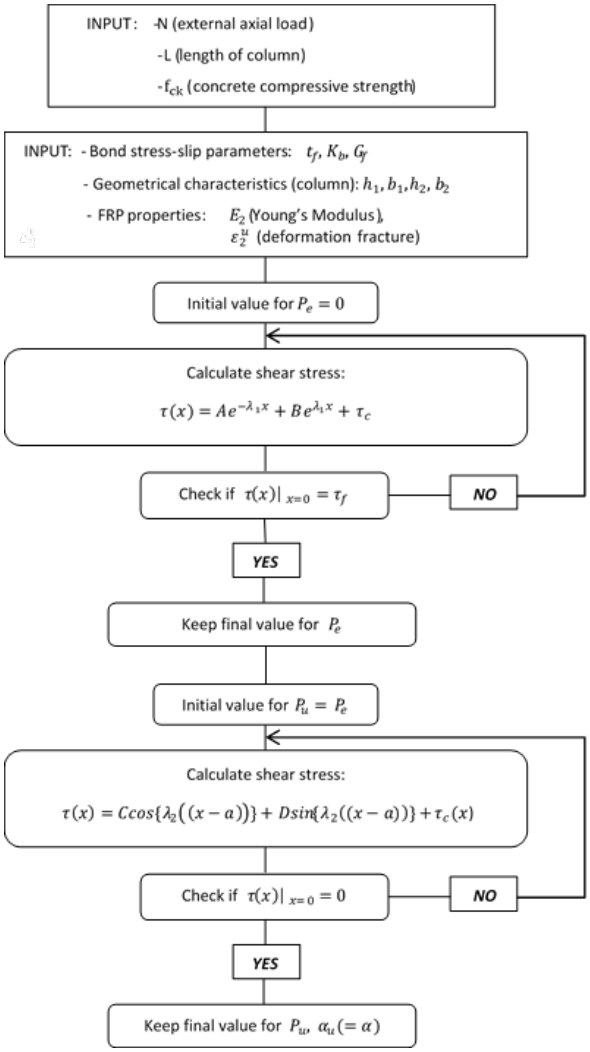

Fig. 3 Calculation of the Interface capacity by iterative method

3.5 Experimental verification

A database of 15 specimens (RC column) from the aforementioned specimens was assembled in order to verify the analytical equations. They were retrofitted with FRP jackets (carbon or glass), with different characteristics and total thickness. Thereafter, for each column, the iterative process described in Section 3.4 was used to find the interfacial stresses together with normalized strain of the FRP along the columns, both for ultimate experimental load and debonding load.

Due to the heterogeneity of specimens, sample was divided into four groups. The first group (Group A) consists of two columns of square cross section (*300x300mm*) strengthened with fiber glass (GFRP) with different total thickness and normalized axial compressive load level equal to 0.14 (v = 0.14). The second group (Group B) (7 specimens) consists of columns with the same section (300 × 300 mm) strengthened with carbon fiber (CFRP) differing in concrete compressive

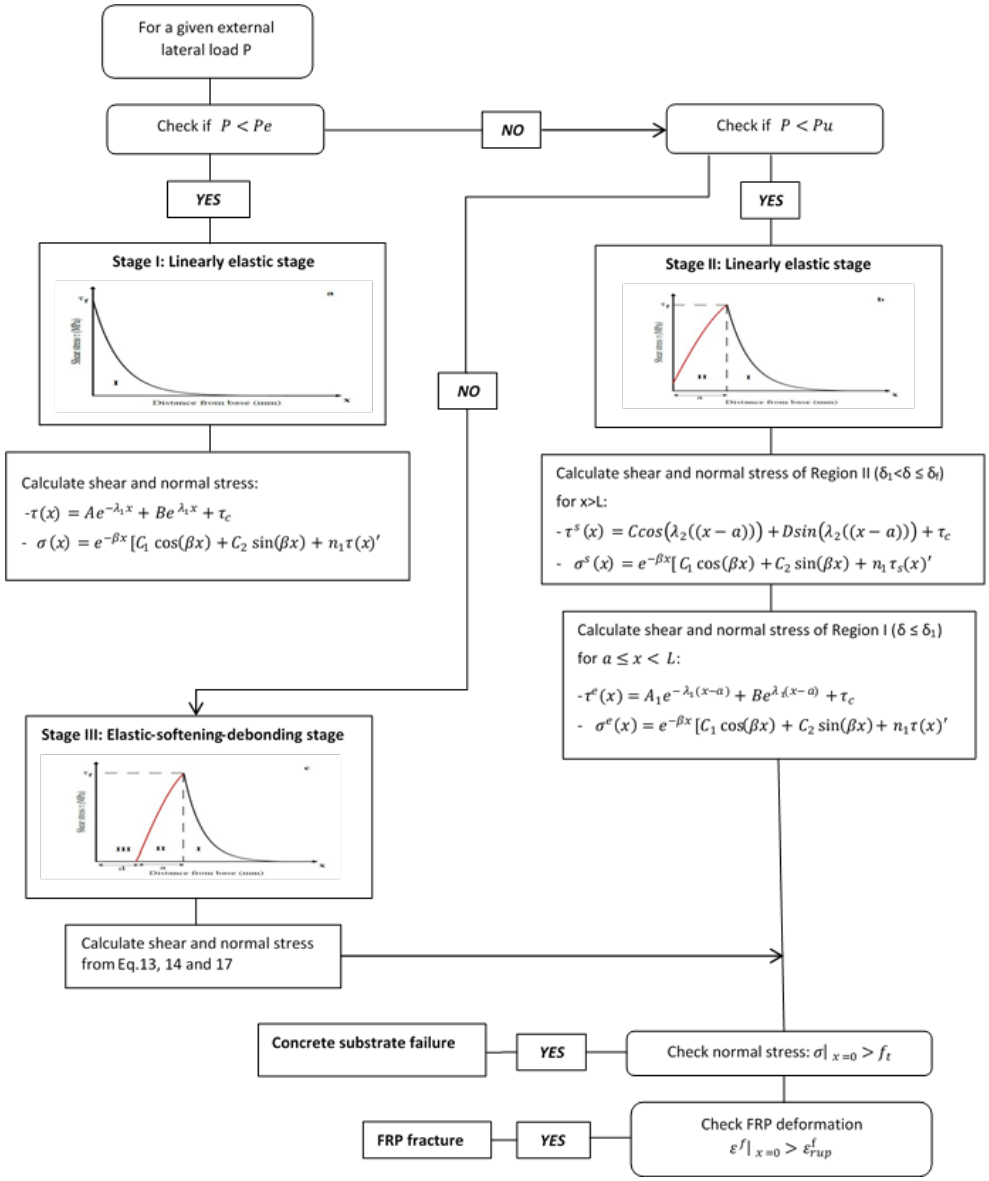

Fig. 4 Calculation of Shear and Normal Stress diagrams and interface failure mechanisms

strength (3.7-27.3 MPa). There was also variation in normalized axial compressive load: specimen C14-D-C has v = 0.12, C22-D-C has v = 0.4 and the rest of them v = 0.14. The third group (Group C) (4 specimens) consists of columns with square cross-section (300 × 300 mm) reinforced with carbon fiber (CFRP) as in group B except that the edges of the columns at the base are placed steel angle profiles. Particularly in two of them, the steel angles were anchored to the foundation of columns with bolts to further increase the flexural strength of the specimens. There is difference in the compressive strength of concrete (14.9-17.3 MPa) and in normalized axial load. Finally, the fourth group (Group D) consists of 3 columns of 200 × 200 mm cross section. The specimens are

retrofitted with carbon fiber (CFRP).

The purpose of this categorization in groups is to clarify which of the variables mentioned above affects the development of internal forces in the concrete-FRP interface and the level of influence. Group A consists of two specimens (C1-S-G ,C4-S-G) of 2200 mm long and square section 300 × 300 m retrofitted with GFRP sheets (C1-S-G with total thickness t_{tot} = 1.92 mm and volumetric ratio $\rho_f = 0.0256$ and C4-S-G with total thickness t_{tot} = 0.96 mm and volumetric ratio $\rho_f = 0.0128$). The compressive strength and tension strength is similar (f_{ck} = 20.8 and 16.8 MPa and f_t = 2.281 and 1.978 MPa respectively). The Young's Modulus of the GFRP is E_f = 80.7 Gpa. The experimental results show that for specimen C1-S-G the maximum horizontal force is F_{max} = 62.45 kN while on C4-S-G is F_{max} = 55.07 kN. According to the analytical solutions, the maximum external force in which debonding in the column-FRP interface occurs (*Stage III*: *Elastic-Softening-Debonding Stage*) is P_u = 89.8 kN (C1-S-G) and P_u = 72.74 kN (C4-S-G). These analytical findings confirm that the failure did not occur from premature detachment of the FRP from the column.

In Fig. 5(a) it is observed that the shear stress is similar at column's base (τ = 4,6 MPa) (x = 0), while the maximum value of (τ_f = 8 MPa) occurs at the same point at a distance of about 30 mm from the base. In addition, for both cases, the stresses are zero at approximately 150 mm from the base meaning that from this point onwards there is no slippage at the interface and both materials are in full contact. So, an increase of the thickness of the retrofitting material (FRP) has negligible influence on the variation of the internal forces.

Fig. 5(b) shows the normal stresses along column-FRP interface calculated by Eq. (17). It is observed that the normal stress in specimen C4-S-G is smaller than specimen C1-SG at the base of the column due to lower total thickness of FRP. Finally, it is noted that in all cases after a 150mm length strip the propagation of interfacial slippage ceases to exist.

Group B includes six specimens with same height and square sections as group A. They are all retrofitted with CFRP sheets (total thickness t_{tot} = 0.44 mm and volumetric ratio $\rho_f = 0.00587$). The Young's Modulus of the CFRP is E_f = 390 GPa. Apart from C14-DC and C22-DC, the compressive strength of concrete and the axial compressive external load of the columns are equal.

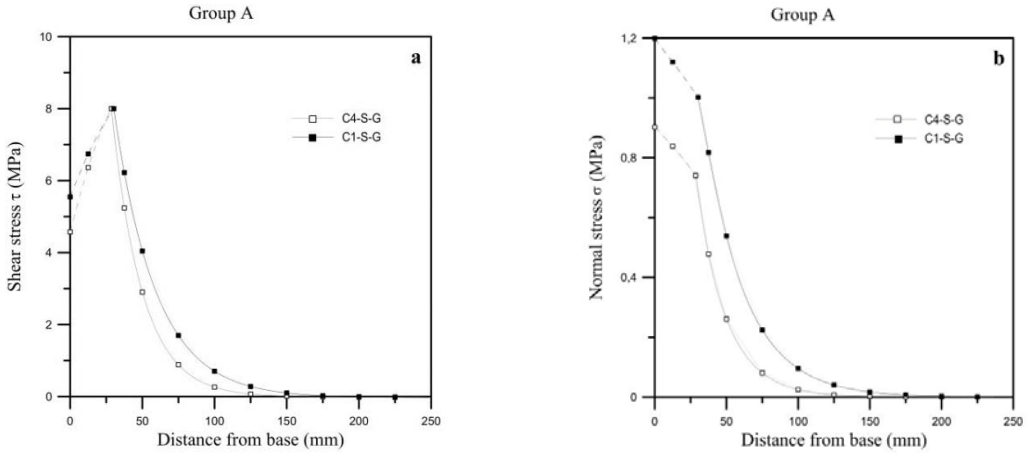

(a) Interfacial shear stress–slip relationship (b) Interfacial normal stress–displacement relationship

Fig. 5 Interfacial stress distributions along FRP–concrete interface for Group A

Their main difference is the maximum moment observed at their base (due to the different conventional longitudinal reinforcement).As shown in Fig. 6(a) in the first two experiments (C10-SC and C13-SC), having smooth longitudinal reinforcement and bearing less moment, the shear stress diagram of them coincides and the maximum value is displayed at a position 20 mm higher from the base. The following two specimens (C7-DC and C8-DC) with deformed longitudinal bars exhibit maximum shear stress at a distance equal to 40 mm from the base and has almost twice the relative slip in relation to the previous two. The columns C14-DC and C22-DC finally are in an intermediate situation. In any case, at a distance longer than 200 mm from the base, there is no slippage at the interface and the two materials are in full contact.

Specimens C10-SC and C13-SC have value 0.25 MPa while C7-DC and C8-DC have a value of about 0.28. Finally specimens C14-DC and C22-DC have intermediate values. It is concluded therefore that the differentiation in terms of longitudinal conventional reinforcement does not substantially affect the development of normal stresses and the failure of the concrete substrate.

Group C consists of four specimens from the database with 2200 mm height and square section 300 × 300 m retrofitted with CFRP sheets (total thickness t_{tot} = 0.44 mm and volumetric ratio ρ_f = 0.00587) and also strengthened with steel angles with anchorage to the concrete foundation (*Type* "*A1*") or without (*Type* "*A2*"). The compressive strength and tension strength of the concrete varied from f_{ck} = 14.9-27.3 MPa and f_t = 1.1.8-2.7 MPa respectively. The Young's Modulus of the CFRP is E_f = 390 GPa. For the two utmost examples the experimental results show that for specimen C6-S-A2 the maximum horizontal force reaches the value of 63.32 kN while on C11-S-A1 it is equal to 97.53 kN. According to the analytical solutions (neglecting steel connectors influence), the maximum external force (P_u) in which debonding of the Column-FRP interface occurs (*Stage III*: *Elastic-Softening-Debonding Stage*) is equal to 93 kN. This verifies that the experiments failure was not caused by loss of function of the force transfer mechanisms between concrete and FRP sheets for all specimens except for the case of C11-S-A1.

Figs. 7(a)-(b) demonstrate the interfacial shear and normal stress distributions, respectively, for the maximum experimental recorded load $F_{\max}$, measured from the base of the column to the top. It can be observed that for three experiments the interface is in *Elastic-Softening Stage* (*Stage II*)

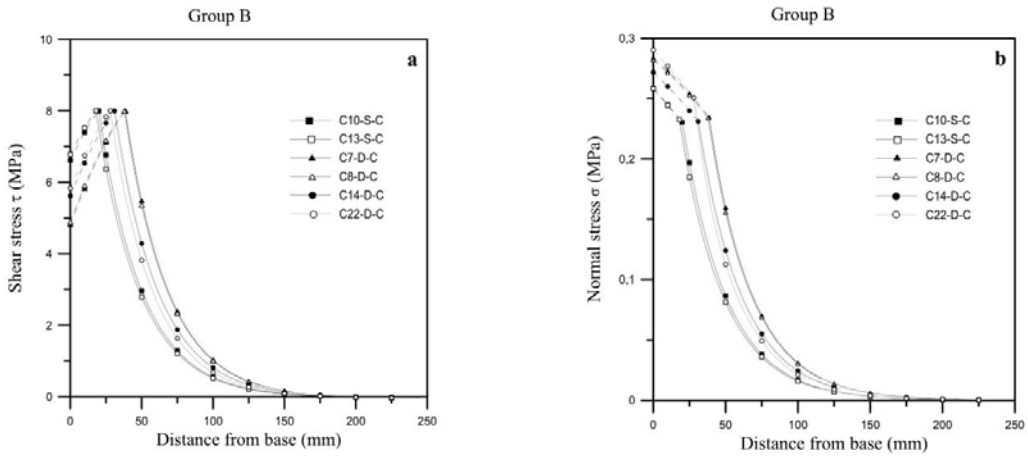

(a) Interfacial shear stress–slip relationship (b) Interfacial normal stress–displacement relationship

Fig. 6 Interfacial stress distributions along FRP–concrete interface for Group B

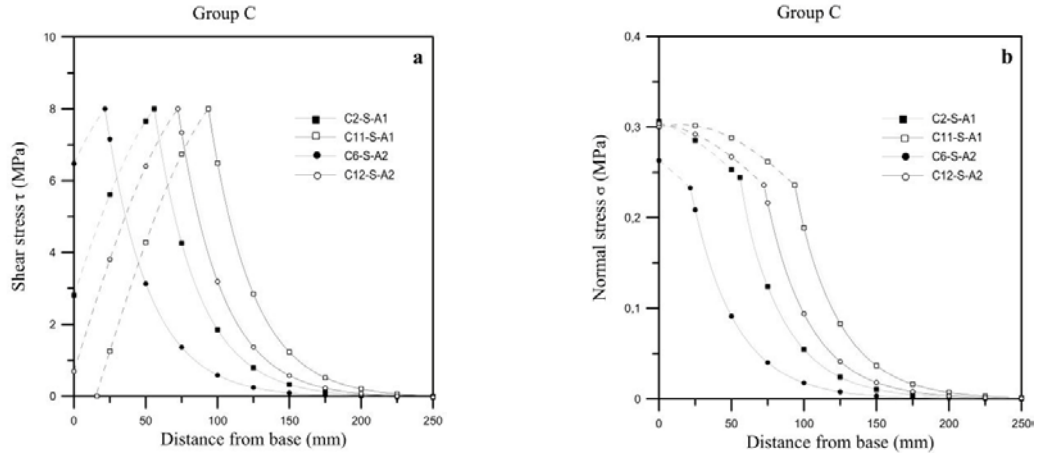

(a) Interfacial shear stress–slip relationship (b) Interfacial normal stress–displacement relationship

Fig. 7 Interfacial stress distributions along FRP–concrete interface for Group C

with the maximum shear stress (τ_f = 8 MPa) recorded at a distance ranging between 21 mm and 90 mm from the base. For C11-S-A1, though, a debonding zone of approximately 15 mm is created. In the experimental process, no failure due to concrete-FRP interface is observed. So, from the algorithm's results it can be assumed that steel profiles placed on the column's base help by shifting the effective length in which debonding may occur over the profiles' length. Finally, no failure on concrete's substrate was observed as seen in Fig. 7(b) as the maximum normal stresses $\sigma(x)$ are significantly smaller from concrete's tension strength.

Finally group D contains three specimens (C4, C5, C6) of 1320 mm height and square cross section (300 × 300 m).The first two columns (C4, C5) were retrofitted with CFRP sheets (total thickness t_{tot} = 0.33 mm, volumetric ratio ρ_f = 0.0066 and Young's Modulus of E_f = 230 GPa)

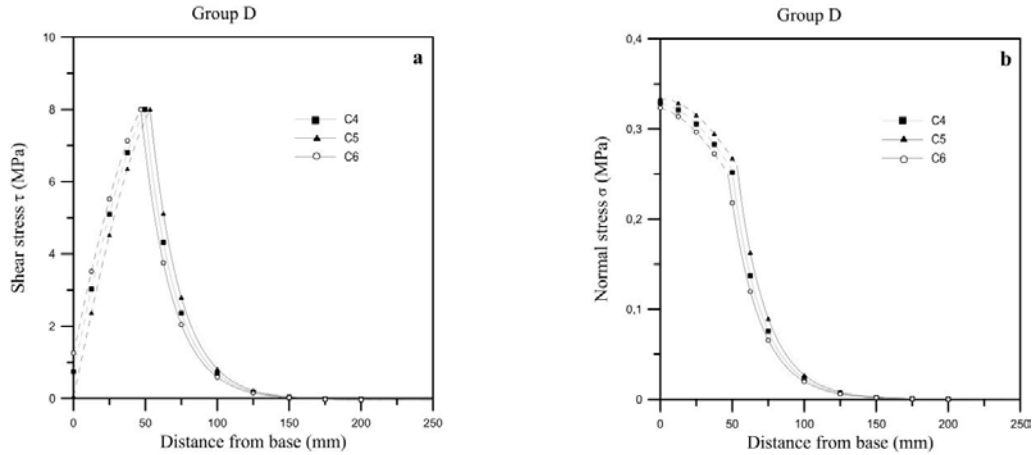

(a) Interfacial shear stress–slip relationship (b) Interfacial normal stress–displacement relationship

Fig. 8 Interfacial stress distributions along FRP–concrete interface for Group D

and GFRP bar embedment. Specimen C6 is only strengthened with CFRP sheets of same thickness. The compressive concrete strength was the same expect of first specimen (for C4 f_{ck} = 46.9 MPa and for the rest is 37 MPa).

As recorded from the experiments the maximum horizontal force F_{max} for specimen C4, C5 and C6 exhibit the values of 53.17 kN, 52.14 kN and 50.16 kN respectively. According to the analytical solutions, the maximum external force (P_u) in which debonding of the column-FRP interface occurs (*Stage III*: *Elastic-Softening-Debonding Stage*) equals to 53.5 kN. This confirms that the failure did not occur from premature detachment of the FRP from the column. The premature detachment is not analytically derived. The code so far can predict debonding zones and stresses. From stresses we can define the loading stage of the FRP itself of the substrate and safely make a conclusion.

As seen from Fig. 8(a), the shear stresses along the FRP-concrete interface are similar with their maximum value (τ_{max} = 8 MPa) concentrated at a distance equal to 50 mm from the base of the columns. As a conclusion, GFRP embedments have negligible effect on the concrete-FRP interface and their use is primarily to increase the displacement ductility of the specimen. Also, for a distance higher than 150 mm from the beginning of measurement, the relative sliding between the two materials disappears. Finally, the normal stresses in Fig. 8(b) (σ = 0.34 MPa at the base of the columns) are similar and after the distance of 150 mm their existence fades.

The effective zone of the FRP is approximately 150 mm (60% of the total length) in the majority of the cases studied. In this length the load transfer exists. The length in which the maximum stresses are noticed is smaller and varies from 10 to 20% of the total length according to cases.

4. Results and discussion

The investigation's conclusions are summarized in a rather qualitative manner in order to explain the interface response based on performance criteria. This part pf the paper is considered to be a helpful tool for practitioners and scientists to understand the mechanisms and functions of each composite technique and scenario and help them choose suitable criteria to evaluate their design. The codes' provisions are a useful tool that is furtherly discussed here.

Firstly, it was observed that strengthening with fiber reinforced sheets leads to increased confined concrete strength, as found in previous research. Also, the increase of confinement causes an increase of the maximum lateral load that the column can bear. The results indicate that by increasing the characteristic strength f_{ck}, a decrease of the maximum normalized horizontal load ρ_{hor}^{max} is appeared, as expected.

Since CFRP's strength is higher, in order to obtain the same results in terms of flexural retrofitting with GFRP strengthening a higher amount of sheet is needed, fact that is confirmed by the dataset's results (Fig. 9(a)). Regarding the maximum displacement and the displacement index I_δ^1, the glass fibers (GFRP) contribute positively in a range of 16-40% and 27-48%, respectively, since the material's failure strain $\varepsilon_{f,u}$ is higher than that of carbon. Concerning displacement ductility (μ_δ), columns retrofitted with GFRP ranged in greater values than the ones strengthened with CFRP (increase of 26-35%) (Fig. 9(b)).

Aiming at flexural strengthening carbon textile reinforced mortar (TRM C) and glass textile reinforced mortar (TRM G) strengthening systems produced similar results (Fig. 9(c)). Carbon TRM tends to increase the compressive concrete strength up to 50% in comparison to TRM G (Fig.

9(a)). In order to increase the ultimate displacement, TRM C was considered more effective since it reached the same ultimate displacement (δ_{max} = 124 mm) but no failure compared to the columns containing TRM G. In terms of displacement ductility TRM C developed *10%* higher displacement ductility levels than TRM G.

By comparing the results of columns strengthened with CFRP and columns with TRMC, it was proved that the TRMC exhibited greater flexural strength index I_μ in a range of 3.6 up to 5.6% (Fig. 9(c)). Regarding the increase in displacement corresponding to the first failure- as defined previously- it seems that in specimens without lap-splices the TRMC has higher contribution than CFRP (52% increased displacement), while in specimens with lap-splices the CFRP contributed in augmenting displacement at a level equal to 16% (Fig. 9(d)). Examining the maximum displacement, in specimens without lap-splices, the TRMC contributes more increasing displace-

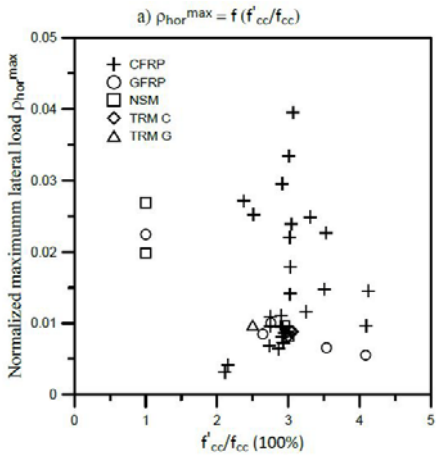

(a) Maximum normalized lateral load dependence on f_{cc}'/f_{cc}

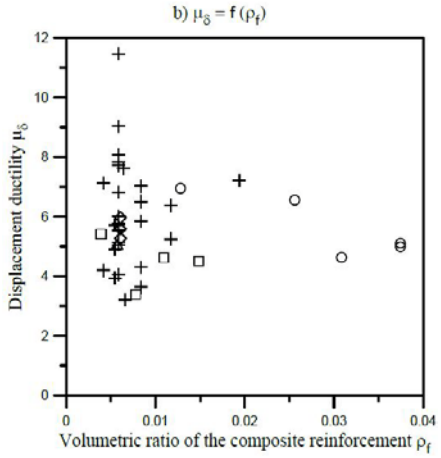

(b) Displacement ductility dependence on volumetric ratio of the composite reinforcement

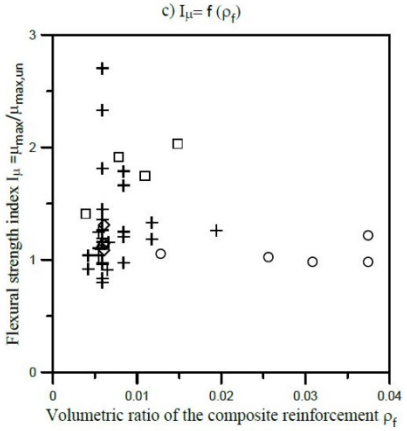

(c) Flexural strength index I_μ dependence on volumetric ratio of the composite reinforcement

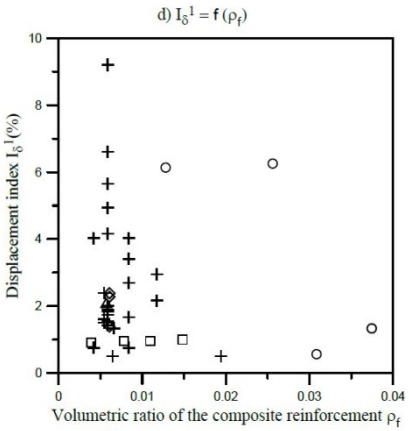

(d) Displacement index I_δ^1 dependence on volumetric ratio of the composite reinforcement

Fig. 9 Dependence of indexes on mechanical characteristics of columns

ment up to 48%. In these specimens both materials demonstrated similar behavior, so the main mechanism that defined the response is the existence of lap-splices. Overall, TRM C exhibited greater values of displacement ductility than CFRP and similar results were recorded between the two materials for enhancing the concrete's compressive strength (Figs. 9(a) and (b)).

Columns with glass fiber composites (GFRP) exhibited three times higher increase in displacement index I_δ^1 and 29% increase in displacement ductility μ_δ compared to columns strengthened with glass textile reinforced mortar (TRMG), since the material corresponds to higher failure strain $\varepsilon_{f,u}$.

Near surface mounted FRP bars (NSM) did not contribute in increasing the displacement in which the first failure is developed and in displacement ductility (Figs. 9(b) and (d)). However, they contributed significantly in increasing the maximum lateral load and maximum moment that the column can undertake (40-90%) (Figs. 9(a) and (c)), making its use an effective flexural strengthening technique.

Composite laminates did not help in increasing the displacement index I_δ^1, the maximum displacement and the displacement ductility. However, laminated are proven to be capable of increasing the maximum moment achieved.

Transverse embedded bars placed in the middle of each side of the column led to increased maximum displacement and ductility. At the same time, the strength for confined concrete and maximum moments is not increased (Figs. 9(a)-(c)).

Steel profiles placed along the corners at the base of each column are proved to have no special effect on confinement and ductility and prevent the full development of maximum displacement and displacement in which the first failure is formed. However, they work favorably in obtaining a

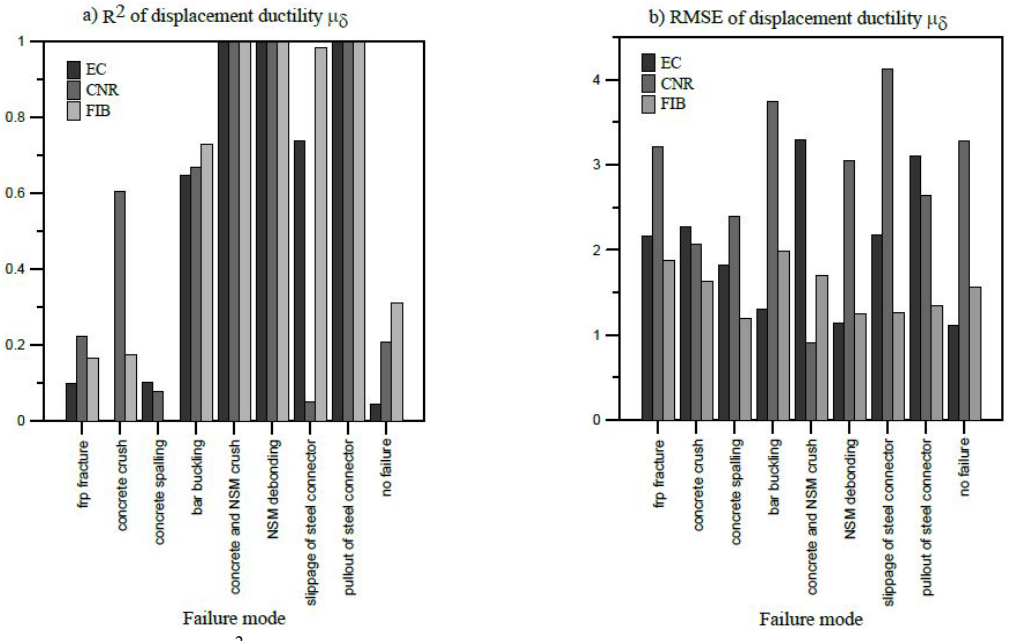

(a) R^2 (b) RMSE

Fig. 10 Bar chart of statistical indexes for displacement ductility μδ for every type of failure and design code (EN 1998-3, CNR, *fib*-Bulletin)

higher level of maximum moment (49% increase). The reason of this notation is attributed to the increased elements' stiffness caused by the installation of steel profiles which prevents it from forming a premature plastic hinge zone.

By analysing the provisions of international standards and codes (EN 1998-3 2005, CNR 2004, *fib*-Bulletin No. 56 2010) R^2 coefficient is extracted. Results show (Fig. 10(a)) that for FRP fracture type of failure, the Italian code (CNR) provides more accurate outcomes, followed by *fib*-Bulletin and Eurocode EN 1998-3. Furthermore, for a concrete spalling type of failure the respective ranking arose differently. In this case Eurocode EN 1998-3 fits better to the experimental results, followed by the CNR and *fib*-Bulletin codes.

The distribution of errors between the results of codes and experiments were examined by using the coefficient *RMSE*. Root of the mean squared error values and the corresponding bar charts (Fig. 10(b)) showed that for FRP fracture and concrete spalling type of failures *fib*-Bulletin code delivers less distribution of errors, followed by Eurocode EN 1998-3 and the CNR code.

In order to identify the code that provides the most conservative results regarding displacement ductility calculations, estimator plots are used. The significant line (ideal estimator) is also known as identity line. The identity line has a slope of 1, meaning that it forms a 45 degree angle with the horizontal and vertical axis. The data correspond to a value of ductility predicted by the design codes on the horizontal axis and the respective experimental value on the vertical axis. If the data create an estimator line that is located above the ideal estimator, the code predicted lower levels of ductility than the experimental values, thus the code is considered conservative. In contrast, if the data emerge below the ideal estimator, the miscalculation according to the design code can result to unexpected failure for specific performance criteria. It is observed that CNR code's provisions are the most conservative. Respectively, the estimator between experiments' and *fib*'s Bulletin ductility results appear under the ideal estimator more often than the other codes' results.

Fig. 11 indicates that displacement ductility in columns that failed due to FRP fracture was calculated successfully by CNR code, while *fib*-Bulletin did not effectively predict the ductility in almost half the specimens. Also, it is worth noting that ductility was efficiently approximated in most cases by EN 1998-3. It can be observed that FRP fracture type of failure is developed for displacement ductility (μ_δ) levels surpassing value of *3*. The group of columns that failed due to FRP fracture includes mainly strengthening systems with FRP sheets, some with embedment of lateral bars made of composite materials and some with steel profiles at the corners. Specimens' C1-S-G and C4-S-G (Realfonzo and Napoli 2009) response containing GFRP sheets were overestimated by EN 1998-3 and *fib*-Bulletin and underestimated by CNR code. In contrast, specimen's response L0_M4G (Bournas *et al*. 2009) with TRMG was underestimated by all the codes' provisions. For specimens retrofitted with steel profiles and/or CFRP sheets CNR code estimated the most conservative values of ductility and *fib*-Bulletin the least. None of the codes takes under consideration the steel profiles in the columns' corners, thus they are expected to predict lesser values of displacement ductility. All three codes' ductility values for retrofitting system containing CFRP sheets and lateral bar embedment were lesser than the experimental, even though they did not account the existence of lateral bar embedment which provide higher confinement levels. Moreover, two lines were drawn representing 20% deflection of the ideal estimator. It is noted that most of the data are included in the range the two lines create, which means that in most cases the design codes estimate ductility values accurately with a 20% deflection. It is worth noting that most of the data located between the deflection lines correspond to Eurocode's EN 1998-3 and *fib*'s Bulletin estimations.

Regarding failure caused by concrete crush, codes EN 1998-3 and CNR predicted sufficiently

the ductility with only one exception for EN 1998-3 (C17-S-C (Realfonzo and Napoli 2009)). Code *fib*-Bulletin developed overestimated and underestimated predictions that led to inconclusive results concerning the code's evaluation. Like FRP fracture, concrete crush failure is developed for displacement ductility levels surpassing value μ_δ = 3. Unretrofitted columns and columns with CFRP sheets are shown in Fig. 11. Code *fib*'s Bulletin predictions overestimate ductility in both unretrofitted columns (C16-S (Realfonzo and Napoli 2009), C2 (Wu *et al*. 2008)), while Eurocode's EN 1998-3 only in one note of C2 specimen (Wu *et al*. 2008) which has no lap-splices and higher longitudinal and transverse reinforcement ratio. Furthermore, strengthened columns' ductility was underestimated in most cases, but specimen C17-S-C (Realfonzo and Napoli 2009) reached lower levels of ductility than Eurocode's EN 1998-3 and *fib*'s Bulletin predictions. The majority of the data were located between the *+20%* and *-20%* deflection lines and belonged mainly to Eurocode's EN 1998-3 and *fib*'s Bulletin provisions, meaning that the design codes estimate ductility values effectively with a 20% deflection.

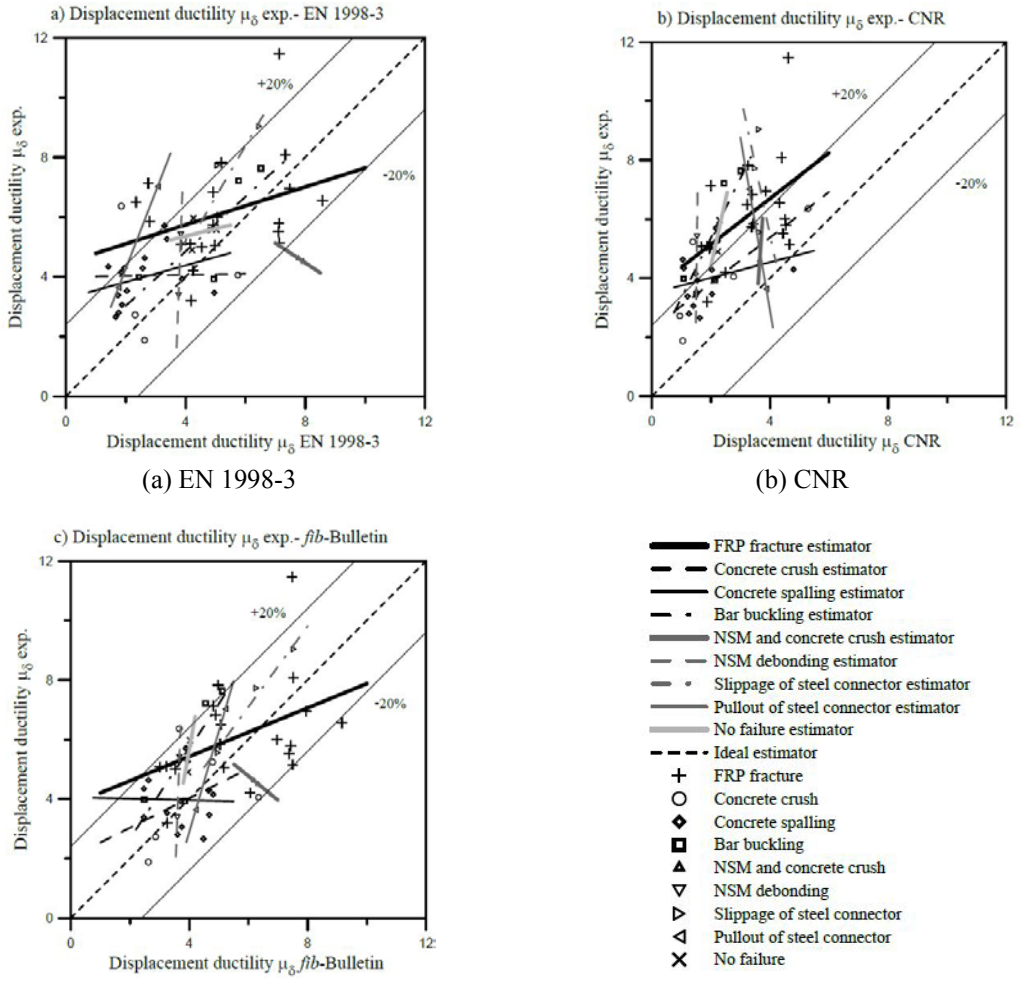

Fig. 11 Estimator charts for every type of failure for code

Concerning columns that failed due to concrete spalling, results showed that codes CNR and EN 1998-3 estimated ductility values lesser than experimental. However, the data are located rather far from the ideal estimator, which indicates safe but not necessarily accurate results. Additionally, *fib*'s Bulletin estimations resulted in some acceptable but also in some risky results. Nevertheless, concrete spalling failure is exhibited in specimens with ductility values equal to *2* or higher. In Fig. 11 it is also shown that unstrengthened columns calculated by codes EN 1998-3 and CNR were expected to develop lower values of displacement ductility, while that occurred to only 40% of those specimens according to *fib*'s Bulletin provisions. Column C33-D-C (Realfonzo and Napoli 2012) was the only one strengthened with sheet composites that was predicted to achieve ductility $\mu_\delta = 4.8$ according to CNR code and $\mu_\delta = 4.67$ according to *fib*-Bulletin, while it reached $\mu_\delta = 4.3$ according to experiments. The fact that the design codes do not take into account the lateral bar embedment's influence is the reason why they all predicted lower ductility values than the experimental. More than half the data are included between the deflection lines with most of them corresponding to Eurocode's EN 1998-3 and *fib*'s Bulletin predictions.

All three codes (EN 1998-3 2010, CNR 2004, *fib*-Bulletin 2010) effectively predict displacement ductility in columns that failed due to longitudinal bar buckling. It's worth noticing that CNR code's values are located once again above but far from the identity line, while in this type of failure Eurocode's EN 1998-3 predictions are the closest to the ideal estimator making it the most accurate code. All columns experienced bar buckling in ductility (μ_δ) level of 4 or greater. The codes estimated lower values of ductility for the unstrengthened column L0_C (Bournas *et al*. 2009) and all the specimens retrofitted with CFRP sheets except L0_R2 (Bournas *et al*. 2009), which didn't have lap-splices, for EN 1998-3. Regarding specimen PCL-1 (Sadone *et al*. 2012) which was strengthened with CFRP sheets and laminates the codes estimated lower ductility levels as well. Composite laminates are not taken into consideration in any of the codes' provisions.

In Fig. 11 the estimator plots for columns that did not reach failure and specimens which failed due to NSM and concrete crush, NSM debonding, slippage and pullout of steel connectors at the base are also demonstrated. Since the sample is inadequate, the results are unreliable. For the sake of brevity, these results are not analytically discussed in this section. However, it is worth noticing that NSM bars and steel profiles at the base of the elements are not taken into account in codes' provisions for calculating the displacement ductility. In general, CNR code is proved to be the most conservative, while *fib*-Bulletin is the most accurate. Finally, CNR code is considered the most conservative and *fib*-Bulletin the least.

The current design codes lack in describing analytically the response and type of failure in the interface between columns and retrofitting material, depending on the type of strengthening technique and performance design. This is significant because premature failure due to debonding is a very common type of failure in FRP strengthened elements. In the current study, an analytical description of this phenomena is addressed by calculating the internal stresses along the interface. The results from this analytical approach are limited to columns with FRP sheet confinement. Different types of strengthening techniques are subjected to future research.

From the exported results, it is concluded that the use of steel connectors in the base of columns apart from strengthening purposes, also helps preventing debonding of FRP sheets and eventually premature failure. As in the experimental process only FRP fracture is observed it is proven that steel connectors helped to shift the maximum stress concentration range in the interface above them and prevent the debonding area which was observed from the analytical solution.

5. Conclusions

A comparison between composite materials and retrofitting systems is conducted. It is noted that design codes do not provide recommendations regarding the most suitable technique for each desired retrofit. Moreover, there are no regulations and distinctions regarding failure modes among different performance levels and strengthening system.

In every retrofitting system the composite material used is found to be a very important factor regarding to the efficiency of the retrofitting element.

The effect of confinement was distinctively significant in the response and behavior of retrofitted concrete columns when subjected to seismic loading in terms of strength, ductility and load and deformation capacity as found in previous research. The new element emphasized by this study is the failure every retrofitting system exhibits depending on the different performance level.

Results show that the conventional reinforcement doesn't have a significant contribution in the overall response of the retrofitted element. Though in cases of lap-splices, it is derived that they can act as an additional parameter to augment the displacement capacity in combination with a suitable retrofitting FRP sheet.

Finally, an algorithm based on non-linear slip-stress law is transformed for cases of RC columns strengthened with FRP sheets. This investigation results in defining the sub-region in which the failure mode initiates and the length in which the phenomenon is developed.

It is noted that the usage of steel profiles at the column's base can contribute in terms of shifting the length of the zone in which debonding of the FRP may be developed. Consequently the length in which stress concentration may occur is eventually located above the profiles. Nevertheless, in all the cases which did not include steel profile retrofitting, the algorithm's results were in good agreement with the experimental observations.

References

Bizindavyi, B. and Neale, K. (1999), "Transfer lengths and bond strengths for composites bonded to concrete", *J. Compos. Construct.*, **3**(4), 153-160.

Bournas, D., Triantafillou, T., Zygouris, K. and Stavropoulos, F. (2009), "Textile-reinforced mortar versus FRP jacketing in seismic retrofitting of RC columns with continuous or lap-spliced deformed bars", *J. Compos. Construct.*, **13**(5), 360-371.

Chajes, M.J., Finch, W.W., Januszka, T.F. and Thomson, T.A. (1996), "Bond and force transfer of composites materials plates bonded to concrete", *Struct. J.*, **93**(2), 209-217.

Chalioris, C.E. (2007), "Analytical model for the torsional behaviour of reinforced concrete beams retrofitted with FRP materials", *Eng. Struct.*, **29**(12), 3263-3276.

Chalioris, C. (2008), "Torsional strengthening of rectangular and flanged beams using carbon fibre-reinforced-polymers – experimental study", *Construct. Build. Mater.*, **22**(1), 21-29.

Chen, J.F. and Teng, J.G. (2003), "Shear capacity of FRP-strengthened RC beams: FRP debonding", *Construct. Build. Mater.*, **17**(1), 27-41.

CNR (2004), Guide for the design and construction of externally bonded FRP systems for strengthening existing structures (materials, RC and PC structures, masonry structures), CNR-DT 200/2004, Italian National Research Council, Advisory Committee on Technical Recommendations for Constructions; Rome, Italy.

Elwan, S.K. and Omar, M.A. (2014), "Experimental behavior of eccentrically loaded RC slender columns strengthened using GFRP wrapping", *Steel Compos. Struct., Int. J.*, **17**(3), 271-285

EN 1998-3 (2005), Eurocode 8: Design of structures for earthquake resistance - Part 3: Assessment and

retrofitting of Buildings, European Committee for Standardization; Brussels, Belgium.
fib-Bulletin No. 56 (2010), Model Code 2010 - First complete draft, Volume 2, International Federation for Structural Concrete; Lausanne, Switzerland.
Karabinis, A. (2002), "Reinforced concrete beam-column joints with lap splices under cyclic loading", *Struct. Eng. Mech., Int. J.*, **14**(6), 649-660.
Karayannis, C. and Sirkelis, G. (2008), "Strengthening and rehabilitation of RC beam–column joints using carbon-FRP jacketing and epoxy resin injection", *Earthq. Eng. Struct. Dyn.*, **37**(5), 769-790.
Hadji, L., Daouadji, T.H., Meziane, M.A.A. and Bedia, E.A.A. (2016), "Analyze of the interfacial stress in reinforced concrete beams strengthened with externally bonded CFRP plate", *Steel Compos. Struct., Int. J.*, **20**(2), 413-429.
Panda, K.C., Bhattacharyya, S.K. and Barai, S.V. (2012), "Shear behaviour of RC T-beams strengthened with U-wrapped GFRP sheet", *Steel Compos. Struct., Int. J.*, **12**(2), 149-166
Realfonzo, R. and Napoli, A. (2009), "Cyclic behavior of RC columns strengthened by FRP and steel devices", *J. Struct. Eng.*, **135**(10), 1164-1176.
Realfonzo, R. and Napoli, A. (2012), "Results from cyclic tests on high aspect ratio RC columns strengthened with FRP systems", *Construct. Build. Mater.*, **37**, 606-620.
Rousakis, T., Karabinis, A.I. and Kiousis, P.D. (2007), "FRP-confined concrete members: axial compression experiments and plasticity modelling", *Eng. Struct.*, **29**(7), 1343-1353.
Sadone, R., Quiertant, M., Mercier, J. and Ferrier, E. (2012), "Experimental study on RC columns retrofitted by FRP and subjected to seismic loading", *Proceedings of Conference on FRP Composites in Civil Engineering* (*CICE*), Rome, Italy, June.
Sarafraz, M. and Danesh, F. (2010), "Experimental study on flexural strengthening of RC columns with near surface mounted FRP bars", *J. Seismol. Earthq. Eng.*, **12**(1-2), 39-50.
Smith, J. and Teng, J. (2001), "Interfacial stresses in plated beams", *Engineering Structures*, **23**(7), 857-871.
Su, L., Li, X. and Wang, Y. (2016), "Experimental study and modelling of CFRP-confined damaged and undamaged square RC columns under cyclic loading", *Steel Compos. Struct., Int. J.*, **21**(2), 411-427.
Wang, J. (2006), "Cohesive zone model of intermediate crack-induced debonding of FRP-plated concrete beam", *Int. J. Solid. Struct.*, **43**(21), 6630-6648.
Wang, J. (2007), "Cohesive zone model of FRP-concrete interface debonding under mixed-mode loading", *Int. J. Solid. Struct.*, **44**(20), 6551-6568.
Wang, J. and Zhang, C. (2008), "Nonlinear fracture mechanics of flexural–shear crack induced debonding of FRP strengthened concrete beams", *Int. J. Solid. Struct.*, **45**(10), 2916-2936.
Wu, Y., Liu, T. and Wang, L. (2008), "Experimental investigation on seismic retrofitting of square RC columns by carbon FRP sheet confinement combined with transverse short glass FRP bars in bored holes", *J. Compos. Construct.*, **12**(1), 53-60.

CC